Experimental Thermal and Fluid Science 57 (2014) 94–101

Contents lists available at ScienceDirect

Experimental Thermal and Fluid Science

journal homepage: www.elsevier.com/locate/etfs

Spreading and receding characteristics of a non-Newtonian droplet impinging on a heated surface

Joo Hyun Moon, Dae Yun Kim, Seong Hyuk Lee *

School of Mechanical Engineering, Chung-Ang University, Republic of Korea

ARTICLE INFO

Article history:
Received 15 January 2014
Received in revised form 1 April 2014
Accepted 1 April 2014
Available online 18 April 2014

Keywords:
Droplet
Impact
Non-Newtonian
Heat transfer
Receding
Spreading
Contact angle

ABSTRACT

The present study aims to investigate the influence of the Weber number and surface temperature on the spreading and receding characteristics of Newtonian (DI-water) and non-Newtonian (xanthan gum solution) droplets impinging on heated surfaces. The surface temperature was in the range from 25 °C to 85 °C, which is below the Leidenfrost temperature (~300 °C). Using high-speed camera images, this study measured the dynamic contact angle as well as spreading and receding diameters. It also used a modified model to predict the maximum spreading diameter by using the effective viscosity. From the results, the modified model using the effective viscosity was in good agreement with the experimental data in predicting the maximum spreading diameter. In addition, the maximum spreading diameter for a DI-water droplet was larger than that of a non-Newtonian droplet because of the difference in liquid viscosity. In particular, for the Newtonian and non-Newtonian droplets, the dynamic contact angle was almost similar in the spreading regime, but in the receding regime, it substantially changes with temperature owing to the variation of viscosity with temperature. Moreover, the spreading diameter rapidly decreased with the increase in surface temperature in the receding regime in which the change in viscous dissipation energy would be important for the receding motion. Finally, the retraction rates of the Newtonian droplet remained constant with temperature, whereas those of the non-Newtonian droplet increased with temperature, thereby supporting the assertion that the viscosity effect is dominant in the receding characteristics after impact.

1. Introduction

Recently, droplet impacts on solid surfaces have been an important research topic for various applications related to multiphase flows, thermal management, spray coating, corrosion of solid surfaces, and ink-jet printing. A fundamental understanding of dynamic droplet behavior and heat transfer characteristics on a solid surface is thus crucial for determining controllable factors such as surface wettability, impact conditions, and fluid properties [1–5]. In fact, many studies have investigated the droplet impact behavior and heat transfer characteristics for a Newtonian droplet impinging on a solid surface. Roisman et al. [4] studied the spreading and receding characteristics by measuring the spreading diameter and dynamic contact angle (DCA), and they compared the experimental data with the numerical results. In addition, they developed a new model to estimate the DCA. Alizadeh et al. [6] examined the thermal effects on the spreading and receding dynamics of a Newtonian droplet on chemically and mechanically textured hydrophilic and hydrophobic surfaces. Pasandideh-Fard et al. [7] investigated the effects of some important parameters, including the droplet diameter, impact velocity, and thermo-physical properties of a liquid on the heat transfer characteristics during droplet impact. In addition, they developed a cooling effectiveness model to evaluate the thermal characteristics during impact and showed that the impact velocity could enhance the heat transfer. Their model has been widely used to investigate the heat transfer characteristics of droplets impinging on heated surfaces [8–10]. Negeed et al. [11,12] conducted the experiments on dynamic behavior of micrometric single water droplets impinging on heated surfaces with and without superhydrophilic coating by using a high-speed camera. They suggested the empirical correlations for the hydrodynamic characteristics of a droplet and examined the influence of the surface roughness and oxidation layer on the dynamic behavior of a droplet on the surfaces [13]. In addition, the effect of surface condition on evaporation of sprayed liquid droplet was investigated and some empirical relationships for the maximum spread of droplet and the solid–liquid contact time were provided [14].

* Corresponding author. Address: 221 Heuksuk-Dong, Dongjak-Gu, Seoul 156-756, Republic of Korea. Tel.: +82 2 820 5254.
E-mail address: shlee89@cau.ac.kr (S.H. Lee).

http://dx.doi.org/10.1016/j.expthermflusci.2014.04.003
0894-1777/

Nomenclature

a	consistency index
D^*	dimensionless spreading diameter
D_{MAX}	maximum spreading diameter
D^*_{MAX}	dimensionless maximum spreading diameter
d_o	the equivalent droplet diameter [26]
d_x	the measured horizontal droplet diameter
d_y	the measured vertical droplet diameter
n	power law index
t	time
v_0	impact velocity
v_{ret}	receding (retraction) velocity

Greek symbols

$\dot{\gamma}$	shear rate
$\acute{\varepsilon}$	retraction rate
$\acute{\varepsilon}_{32}$	retraction rate at Weber number of 32
$\acute{\varepsilon}_{126}$	retraction rate at Weber number of 126
μ	shear viscosity with time
μ_o	zero shear viscosity
μ_∞	infinite-shear viscosity
ρ	density
γ_{LV}	surface tension between liquid and vapor phases
θ_a	advancing contact angle at maximum spread
θ_e	equilibrium contact angle between a droplet and a solid surface
θ_d	dynamic contact angle

Dimensionless numbers

Re	Reynolds number ($=\rho v_o d_o/\mu_o$)
Re_{eff}	Effective Reynolds number ($=\rho v_o d_o/\mu_{eff}$)
We	Weber number ($=\rho v_o^2 d_o/\gamma_{LV}$)

Recently, interest in non-Newtonian fluids for industrial applications has rapidly increased, and many results have been reported on the heat transfer and dynamic behavior of non-Newtonian droplets [15–23]. The pioneering work of Bergeron et al. [15] incorporated small amounts of a flexible polymer that inhibited the droplets' receding motion and suppressed the rebound without changing the shear viscosity. Later, Moon et al. [20] measured the spreading diameter and DCA for Newtonian and non-Newtonian droplets impinging on unheated solid surfaces. They reported that the evolution of the DCA in the spreading regime was similar for non-Newtonian and Newtonian droplets, whereas in the receding regime, the DCAs of non-Newtonian droplets increased owing to the increase in shear viscosity at lower shear rate.

An and Lee [16,17] examined the impact dynamics of a non-Newtonian droplet on various solid surfaces with different hydrophobicities and suggested a new model for estimating the maximum spreading diameter. German and Bertola [21] discussed the dynamic behaviors of a non-Newtonian droplet that were associated with yield stress and shear-thinning characteristics. They showed that the maximum spreading diameter was affected by the surface wettability and yield stress. Meanwhile, Bertola [24] studied a bouncing droplet of polymer additives to examine the Leidenfrost phenomena of non-Newtonian droplets on a heated surface. Bertola [22] also investigated the impact of a water droplet containing a polymer additive on a hot surface above 100 °C. Bartolo et al. [19] measured the retraction rate of a Newtonian liquid droplet impinging on hydrophobic surfaces for cases with a very high Weber number. Their results demonstrated that the retraction rate of Newtonian droplets rarely depended on the Weber number based on the impact velocity. Even with the many studies [7,9,10,25] that have been reported, there is still a lack of experimental studies on non-Newtonian droplets impinging on a heated surface. Thus, the present study aims to investigate the influence of important factors such as surface temperature, liquid property, and impact velocity on the dynamic behavior of Newtonian and non-Newtonian droplets.

2. Experimental setup

As shown in Fig. 1, a free-fall droplet was detached from a flat-tipped metal needle (30 gage, Hamilton), which was connected to a syringe pump (LSP01-1A, LongerPump). The detached droplet had an equivalent droplet diameter of 2.30 mm ± 0.05 mm, which was estimated from $d_o = (d_x^2 \times d_y)^{1/3}$ [26]. Using the droplet diameter and liquid property, the density of de-ionized (DI) water and xanthan gum liquid can be estimated from the weight measured by a microbalance (AC121S, Sartorius). The impact velocity was controlled by changing the height between the tip of the needle and top of the solid surface. The Weber numbers, which were defined as $\rho v_o^2 d_o/\gamma_{LV}$, were determined to be 32, 64, and 126, for impact heights of 50, 100, and 200 mm, respectively. The present study focused only on the deposition regime under a relatively low Weber number [2,16].

The present study used DI-water and a xanthan solution to prepare the Newtonian and non-Newtonian droplets, respectively. Xanthan gum was mixed with DI-water in different concentrations of 0.1, 0.2, and 0.5 wt.% (hereafter denoted as X0.1, X0.2, and X0.5, respectively). When preparing the xanthan gum solutions, a magnetic stirrer was used to mix DI-water with xanthan gum particles for 24 h, and a vacuum pump was utilized to remove bubbles from the liquid. For the imposed shear rate, the liquid shear viscosity

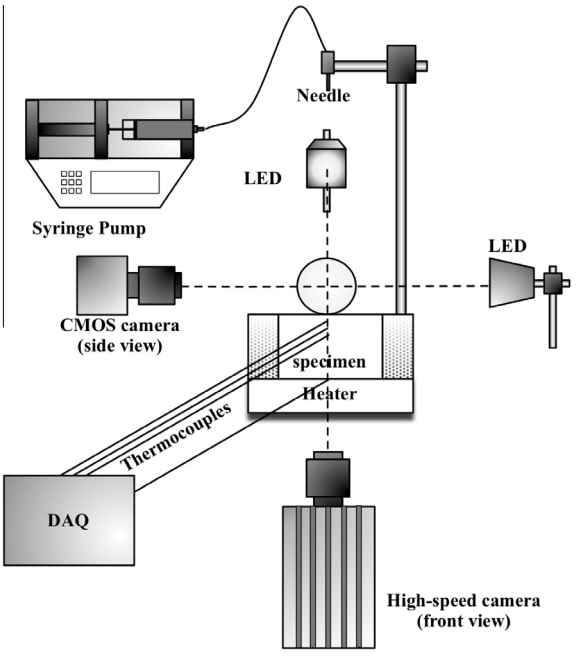

Fig. 1. A schematic diagram of the experimental setup.

was measured using a rotational viscometer (UDS 200, Paar Physica) as shown in Fig. 2. The zero-shear viscosity for the xanthan gum solution was measured at a very low shear rate up to 3×10^{-2}/s and a fixed temperature of 25 °C. To measure the surface tension, we also used a digital surface tension analyzer (DST 60, SEO) based on the well-known Du Noüy ring method [20,27]. Meanwhile, the viscosity and surface tension data were taken from the literature [16,28]. All the fluid properties used in the present study are summarized in Table 1.

To evaluate the surface wettability, it was necessary to measure the equilibrium contact angle (ECA), θ_e, for the DI-water and xanthan droplets deposited on solid surfaces. To measure θ_e, all the captured images were analyzed using the low bond-axisymmetric drop shape analysis (LB-ADSA), which was originally embedded in Image J program using the Young–Laplace equation [29]. According to Table 1, the ECAs are nearly constant, thereby indicating that the effect of particle concentration on the surface tension is very small, whereas the viscosity heavily depends on the particle concentration, as shown in Fig. 2. In particular, the dynamic droplet behavior was visualized using a high-speed camera (HG-LE, Redlake) and Telecentric lens (TEC-M55, Computar) to capture non-distorted images at 4000 frames/s with a 5-W light emitting diode (LED) lamp. The pixel resolution was 17.8 μm/pixel. Moreover, we used a CMOS camera (MI300, Artray) and Telecentric lens (TML-HP lens, Edmund) to ensure axisymmetry. From the captured images, the time evolution of the DCAs (θ_{DCA}) was reported using the Image J program.

A cylindrically shaped copper specimen (99.97% purity) was used as the target solid surface, while the roughness was controlled by polishing the surface with silicon carbide abrasive sandpaper. The average roughness R_a was about 0.05 μm. All the experiments were carried out under well-controlled environmental conditions, i.e., at a room temperature of 23.6 ± 1.0 °C and a relative humidity of 24.7 ± 3.5%, which were measured using a temperature humidity transmitter (TH100, Kimo). The specimen was covered in insulation wool and mounted on a copper block, which was heated using a 100-W coil heater controlled by an AC temperature controller (TPR-2N, Hanyoung). A K-type thermocouple with a response time of 1.0 s was inserted into the coil heater. It was assumed that the heat loss in the radial direction was negligible because the thermal conductivity of the copper was three orders of magnitude higher than the thermal conductivity of the insulation material [30]. Three J-type thermocouples were also embedded in the copper specimen for in situ temperature measurements of the solid surface. All the data were gathered using a terminal block (34901A, Agilent), which was directly connected to a data acquisition system (34970A, Agilent). In this experiment, the surface temperature before impact was maintained at 25 °C, 50 °C, and 85 °C, and the surface temperature deviations were within ±0.5 °C. On the other hand, the droplet temperature remained at 24.2 ± 1 °C. According to previous studies [31,32], the evaporation effect can be ignored because the spreading and receding regimes take place within a very short time frame (~a millisecond) in which the heat and mass transfer are insignificant in the first regime, which occurs approximately 1.0 s after impact [32].

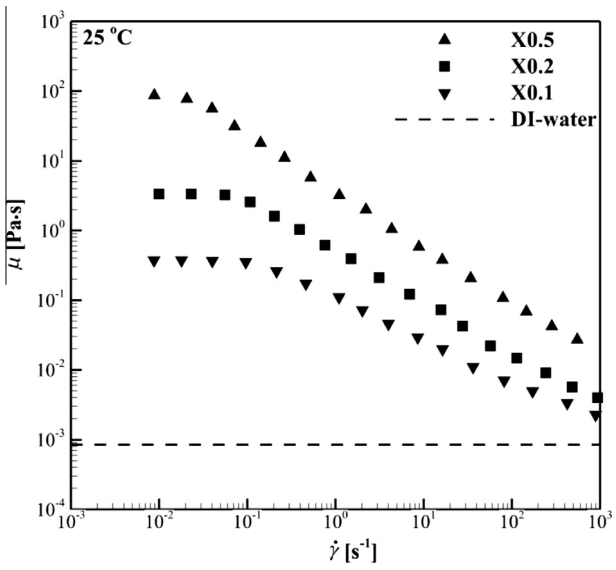

Fig. 2. Measured shear viscosity in terms of the shear rate for water and xanthan gum solutions. The viscosity of DI-water is from Kestin et al. [28].

Table 1
Properties of and equilibrium contact angles for DI-water and xanthan solutions at 25 °C.

	DI-water	X0.1	X0.2	X0.5
μ_o (Pa s)	0.0089 [28]	0.375	3.29	84.5
ρ (kg/m^3)	998	999	999	999
n	–	0.41	0.286	0.209
k (Pa s^n)	–	0.1069	0.785	3.28
γ_{LV} (N/m)	0.072 [16]	0.0707	0.0714	0.0729
θ_e (°)	80.9 ± 1.098	79.7 ± 1.51	79.3 ± 2.48	80.9 ± 2.03

3. Results and discussion

Fig. 3 shows the spreading and receding sequential images of the DI-water and xanthan gum droplets with respect to the surface temperature. After a droplet impinges on the surface, it rapidly begins spreading along the surface until it reaches a maximum spreading diameter and then recedes. Eventually, the final equilibrium state was achieved at t = 0.2 s for all cases. From this figure, the spreading motions between the DI-water and X0.2 are similar until maximum spread, whereas the receding motions are quite different. It is because the difference in liquid viscosity. In fact, the surface energy stored in liquid film after the maximum spread is consumed to generate the kinetic energy required for a receding motion, closely affected by the viscous dissipation energy. The times required for reaching maximum spread are slightly different between the DI-water and X0.2 due to the difference in viscosity. However, those are nearly the same for a given fluid (DI water or X0.2), in spite of the increase in surface temperature. It indicates that thermal effect on dynamic motion of a droplet is not prominent in the spreading regime. This is because the droplet temperature rarely varies for a very short time (~4 ms), as explained previously on the basis of the transient heat conduction theory [33]. In the receding regime, the X0.2 droplet recedes much faster as the surface temperature increases because of the decrease in viscosity, supporting that the thermal effect on the dynamic motion of a droplet cannot be ignored.

3.1. Maximum spreading diameter

Unlike a Newtonian fluid, the shear viscosity of the xanthan gum solution rapidly decreases with increasing shear rate [16,21,34,35]. In general, the power law for shear viscosity variation can be expressed as

$$\mu = K(\dot{\gamma})^{n-1}, \quad (1)$$

where k is the consistency index used in the power-law expression. The dynamic behaviors of a liquid droplet on the surface can be analyzed on the basis of energy consideration in terms of the kinetic

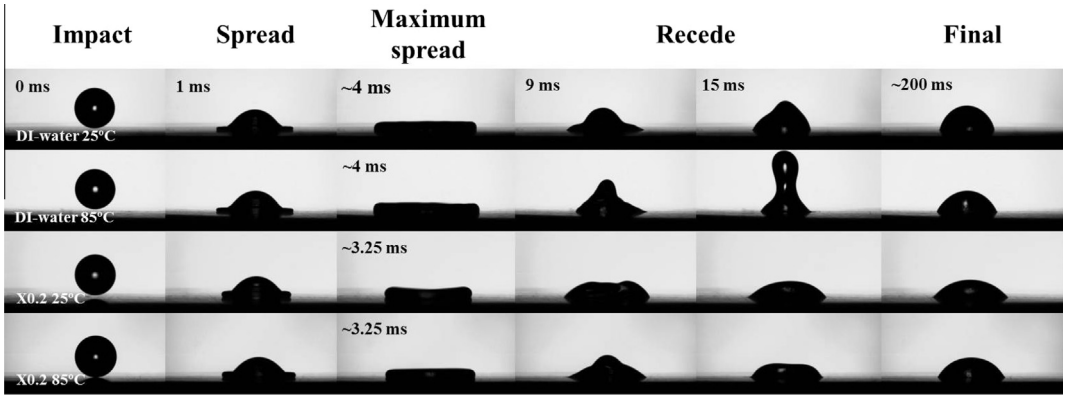

Fig. 3. Time evolution images for DI-water and X0.2 droplets impinging on solid surfaces at We = 64.

(E_K) and surface (E_S) and viscous dissipation energies (E_D) [17,26,36] as follows:

$$E_{K1} + E_{S1} = E_{K2} + E_{S2} + E_{D,SP} \quad : \text{spreading regime} \tag{2a}$$

$$E_{S2} = E_{K3} + E_{S3} + E_{D,RC}, \quad : \text{receding regime} \tag{2b}$$

where the subscripts 1 and 2 indicate the energy before impact and at the maximum spread state and the subscript 3 denotes the energy in the receding regime. The subscripts SP and RC also mean the spreading and receding regimes for viscous dissipation energy, respectively. After impact, the surface energy becomes substantially important toward the end of spreading regime and the kinetic energy related to the inertia force becomes zero ($E_{K2} = 0$) at the maximum spread state. Meanwhile, in the receding regime, the surface energy stored is converted into the kinetic energy required for making a receding motion along the surface. Based on the energy consideration, Ukiwe and Kwok [37] developed a simple model to predict the maximum spreading diameter on flat surfaces on the basis of an energy conservation equation with non-dimensional parameters such as the Weber number and Reynolds number ($=\rho v_o d_o/\mu_o$). The expression for the dimensionless maximum spreading diameter D^*_{MAX} ($=D_{MAX}/d_o$) on flat surfaces is

$$(\mathrm{We} + 12)D^*_{\mathrm{MAX}} = 8 + {D^*_{\mathrm{MAX}}}^3\left(4\frac{\mathrm{We}}{\sqrt{\mathrm{Re}}} + 3(1 - \cos\theta_a)\right). \tag{3}$$

From Eq. (3), the maximum spreading diameter can be estimated by measuring the advancing contact angle at maximum spread. In this study, we used the measured value of the advancing contact angle at maximum spread, θ_a. The advancing contact angle of the DI-water droplets was 95 ± 2.54°, whereas that of the xanthan gum droplets was 97 ± 3.1°.

Fig. 4(a) shows the comparison between the predicted and measured maximum spreading diameters for DI-water and xanthan gum droplets at 25 °C. From this comparison, the Ukiwe–Kwok (U–K) model exhibited a relatively good agreement with the experimental data for a DI-water droplet; there was approximately a 6.71% deviation. This slight over-prediction is attributed to the under-prediction of the viscous dissipation in this model. The maximum error in measuring DCA was ±5° approximately, and accordingly the maximum error of maximum spreading diameter was estimated 3%. For non-Newtonian droplets, however, clear under-predictions (up to 97.1%) can be observed when the original the U–K model was used to predict the maximum spreading diameter. As the Weber number increases, a bigger deviation between the prediction and measurement was clearly observed for the non-Newtonian droplet. This result arises because the original U–K model, which uses only zero shear viscosity, cannot consider the change in shear viscosity during the spread. It also means that

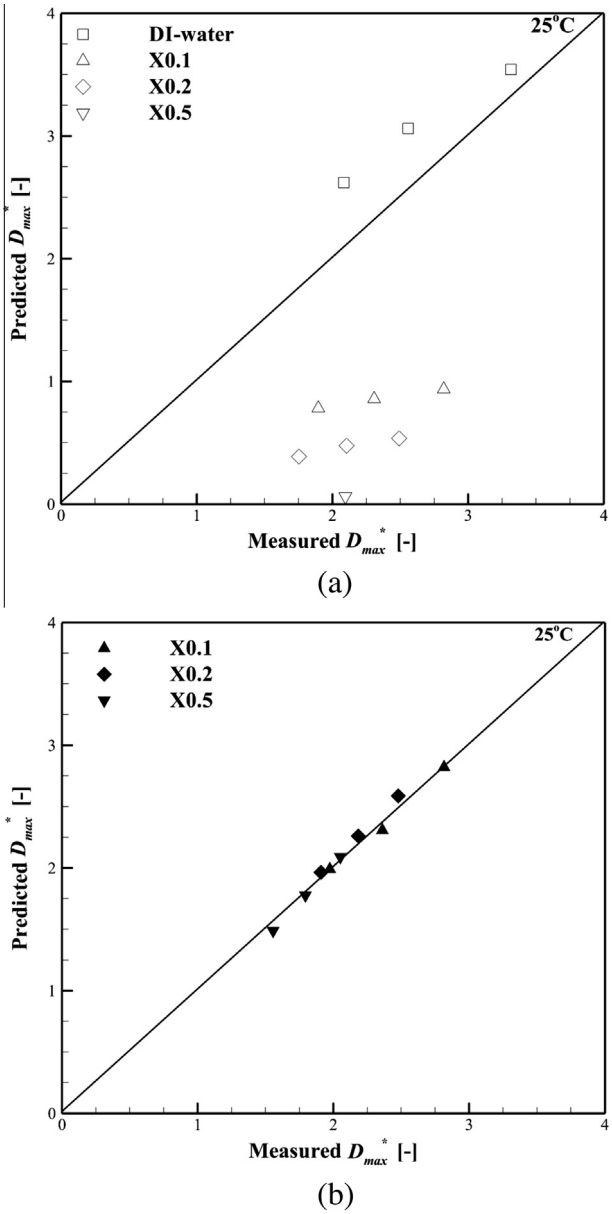

Fig. 4. Comparison between the measured and predicted dimensionless spreading diameters for DI-water and xanthan gum droplets at 25 °C: (a) prediction with [37] and (b) prediction with the modified U–K model [17]. Some cases of X0.5 could not be displayed, as the predicted values were negative.

there is a substantial change in viscosity that heavily depends on the impact velocity. In fact, the shear viscosity of shear-thinning droplets varies continuously according to the shear rate; its value will range from zero shear viscosity to infinite shear viscosity [16,23]. Thus, the shear-thinning behavior must be considered during the spreading regime of the xanthan gum droplets. For better prediction of the maximum spreading diameter, the present study used the effective viscosity, which was originally proposed by An and Lee [17], for considering the variation of liquid viscosity during the impact. The effective viscosity can be expressed as

$$\mu_{eff} = \frac{\mu_0 - \mu_\infty}{1 + k \cdot C\left(\frac{3(D^*_{MAX})^2 v_0}{2d_0}\right)^{1-n}} + \mu_\infty, \quad (4)$$

where μ_∞ denotes the infinite shear viscosity and C indicates the empirical coefficient taken as 6.5 for best fit to the experimental data. The effective viscosity can be used in the deposition regime under the limited conditions such as $We < Re_{eff}^{0.5}$ and $We < 12$ [7]. By substitution of the effective viscosity into the original U–K model, the modified U–K model can be obtained as follows:

$$(We + 12)D^*_{MAX} = 8 + {D^*_{MAX}}^3\left(4\frac{We}{\sqrt{Re_{eff}}} + 3(1 - \cos\theta_a)\right), \quad (5)$$

where $Re_{eff} = \rho v_o d_o/\mu_{eff}$. The numerical results using the modified U–K model are presented in Fig. 4(b). For a non-Newtonian droplet with shear-thinning characteristics, the modified U–K model was in better agreement with the experimental data when compared to the original U–K model. It indicates that the non-linear effect, which is involved in the effective viscosity, should be included in estimating the viscous dissipation energy.

3.2. Spreading and receding behavior

Fig. 5 indicates the dimensionless spreading and receding diameters for DI-water and xanthan gum droplets, respectively, at different Weber numbers. The time required for the maximum spread slightly decreased as the Weber number increased, which is similar to previous results [2,38,39]. Compared to the DI-water droplet, the maximum spreading diameter decreased for non-Newtonian droplets. This difference is because the xanthan gum solutions exhibit a higher viscosity. In fact, the dynamic motion of liquid lamella during the spread is associated with the surface tension force related to wettability, kinetic motion, and viscous force [2,38,39]. Moreover, for We = 32 and 62, the spreading diameter remained nearly constant after 12 s, indicating that the receding motion no longer occurred.

Fig. 6 indicates the dimensionless spreading and receding diameters for DI-water droplets at different surface temperatures. As mentioned previously, thermal dependency of the maximum spreading diameter is very small and the times required for reaching the maximum spread are nearly the same even if the surface temperature is changed. This shows that in the spreading regime, the inertial effect is dominant and thermal effect on the viscous dissipation energy is relatively small. On the other hand, a substantial change of spreading diameter was observed in the receding regime because energy transfer from the surface to the liquid film causes the change in viscosity.

The DCA is generally related to the interfacial dynamics [4,40]. Fig. 7(a and b) shows the spreading diameter and dynamic contact angles for a xanthan gum droplet (X0.1), respectively. In Fig. 7(a), the maximum spreading diameters were nearly identical, and the maximum spread occurred at $t = 3.25$ ms, regardless of surface temperature. This indicates that the variation of a liquid property with temperature is dominant in the receding regime in which the viscous dissipation is relatively more important compared to the spreading regime. As shown in Fig. 7(b), a drastic decrease in DCA was observed until ~9 ms; however, DCAs were nearly identical for different surface temperatures. These phenomena clearly show that the decreasing rate of DCAs is independent of the viscous and surface properties and mainly depends on the inertia force [2]. In addition, the DCAs of the droplet changed rapidly after 9 ms and a substantial dependency on temperature was observed.

For both DI-water and xanthan gum cases, droplets receded faster after the maximum spread because of the rapid decrease in viscosity, which is affected by surface temperature. Fig. 8(a and b), respectively, show the spreading and receding characteristics for the Weber number in terms of solid surface temperatures. Xanthan gum droplets receded faster at higher Weber numbers for all temperatures. In addition, when the impact velocity increased, the droplets receded faster at higher surface temperatures. In the receding regime, the spreading diameter was rarely affected by the surface temperature for relatively low Weber numbers, which are associated with the amount of initial kinetic energy required to

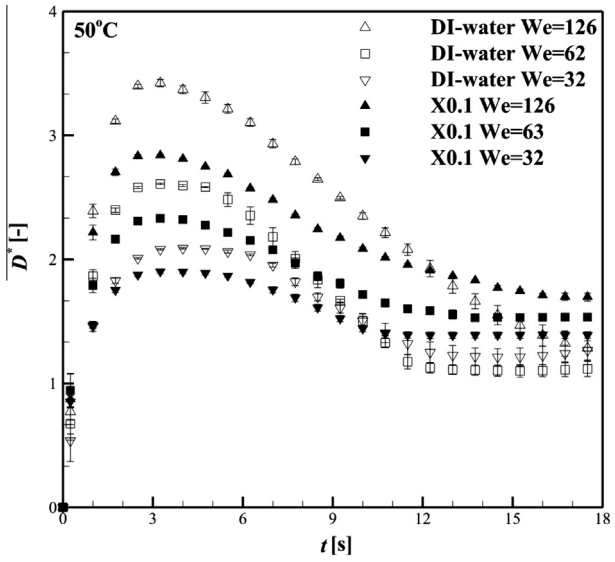

Fig. 5. Measured spreading and receding diameters with respect to the Weber number for DI-water and X0.1 at 50 °C.

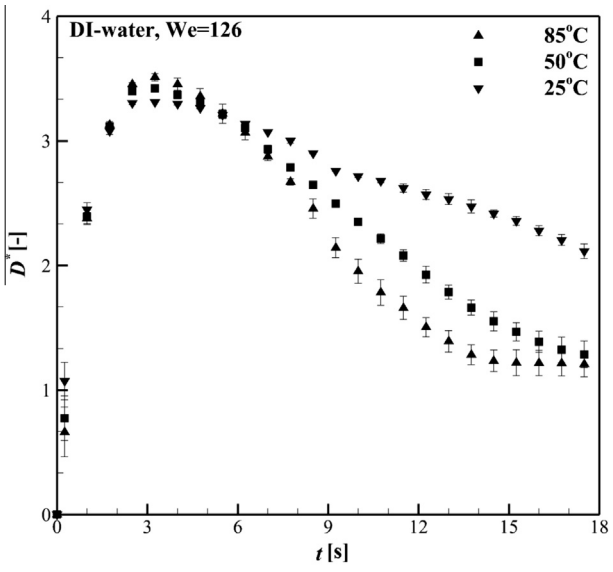

Fig. 6. Measured spreading and receding diameters with respect to the solid surface temperatures for DI-water.

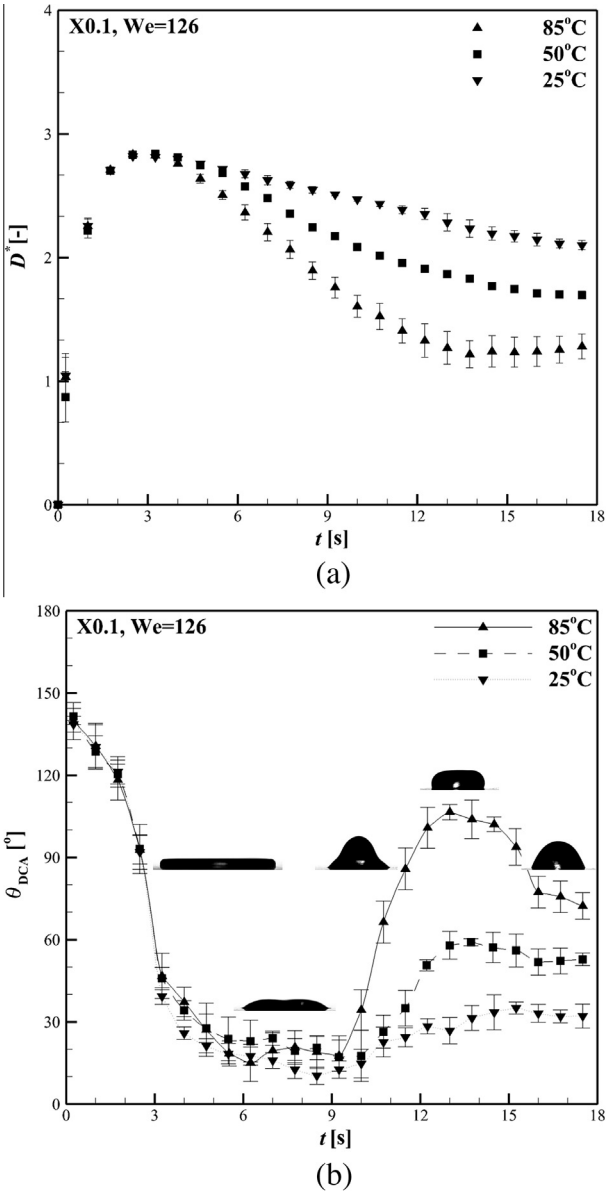

Fig. 7. Measured xanthan gum spreading and receding characteristics with respect to the solid surface temperatures: (a) spreading and receding diameters and (b) DCAs.

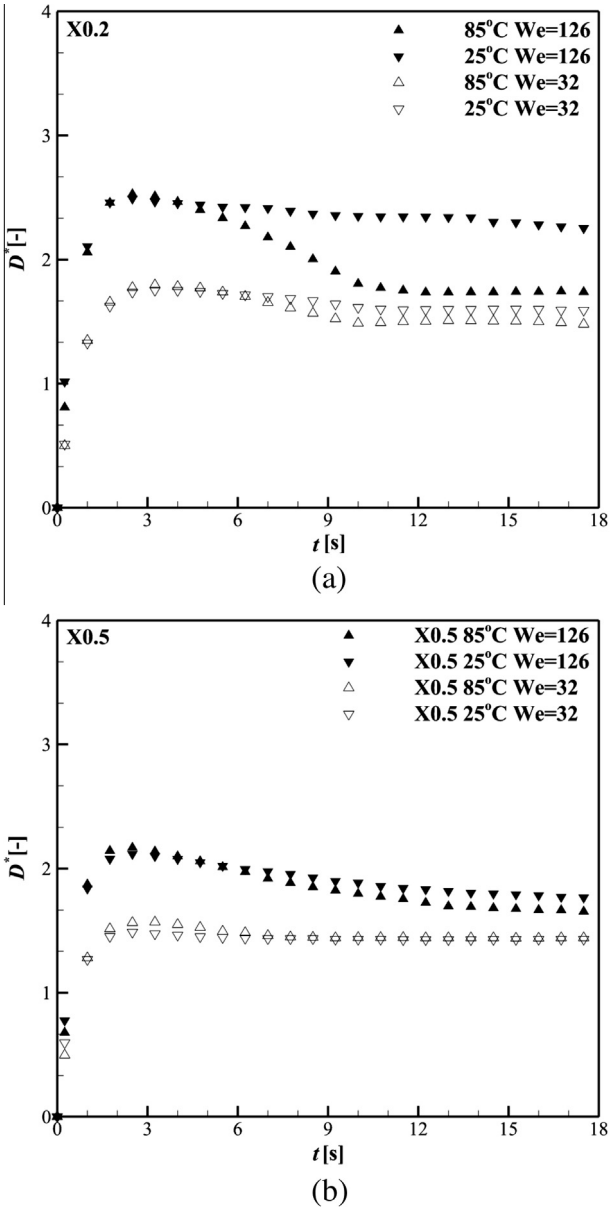

Fig. 8. Measured spreading and receding diameters with respect to the solid surface temperatures and Weber numbers for (a) X0.2 and (b) X0.5.

produce a spreading motion after impact. On the contrary, for We = 126, the spreading diameter remained constant at 85 °C, whereas it rapidly decreased for higher surface temperatures. This indicates that the temperature-dependent change in viscosity significantly affected the receding motion after maximum spread. In particular, for the X0.5 case with higher viscosity, the temperature scarcely affected the variation of spreading diameter, and only a very small variation of the spreading diameter was observed in spite of the increase in the Weber number.

As noted previously, it is clear that the dynamic behavior of a xanthan gum droplet in the receding regime is significantly affected by the mutual interaction between the surface and viscous dissipation energies, which are closely associated with the variation of temperature and impact velocity. To elucidate the role of surface temperature on both the Weber number and xanthan gum concentration of a receding droplet, we adopted the concept of the retraction rate, which was first introduced by Bartolo et al. [19] as $\acute{\varepsilon} \equiv 2v_{ret}/D_{max}$, where $v_{ret} \equiv \max[-\dot{D}(t)]/2$. Fig. 9(a and b) shows the estimated retraction rate with respect to Weber number for different surface temperatures and particle concentrations. According to the results of Bartolo et al. [19], the retraction rate is independent of the impact velocity for a Newtonian droplet. In Fig. 9(a), very similar tendency was observed, i.e., the impact velocity does not affect the retracting motion for both Newtonian and non-Newtonian droplets. For the non-Newtonian droplet case, however, the retraction rate was much lower than that of the DI-water droplet because the shear viscosity of non-Newtonian droplet was much higher than that of DI-water for the entire range of shear rates. In particular, as the solid surface temperature increased to 85 °C, as shown in Fig. 9(b), the retraction rate clearly increased for all Weber numbers and xanthan gum concentrations. For the xanthan gum droplet cases (especially for the X0.1 and X0.2 cases), the retraction rate increased with increasing Weber number, whereas for the case of the DI-water droplet, it remained nearly constant. For the X0.1 case, the increase rate of the retraction rate was 9.7% at 85 °C $((\acute{\varepsilon}_{32} - \acute{\varepsilon}_{126})/\acute{\varepsilon}_{32}$, where the subscript 32 indicates that the Weber number is 32) and that of X0.2 was

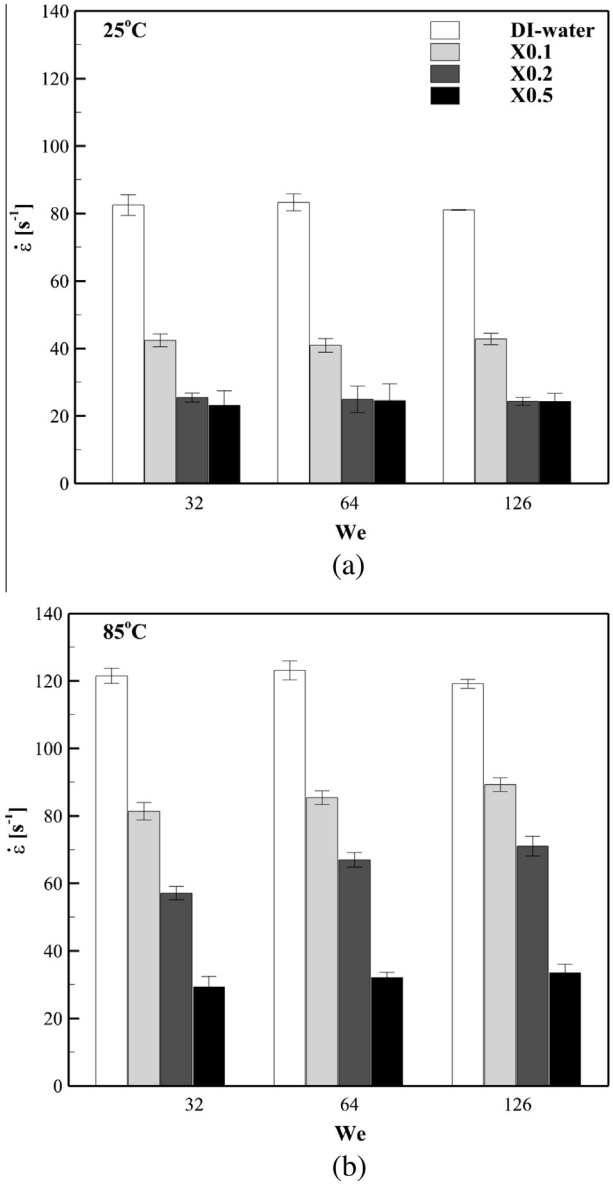

Fig. 9. Retraction rate with respect to the Weber number for solid surface temperatures of (a) 25 °C and (b) 85 °C.

19.6% at 85 °C. For the xanthan gum droplet, the zero shear viscosity decreased by 99.3% when the temperature was increased from 20 °C to 80 °C for the X0.5 case [41], whereas the viscosity of DI-water deceased by only 64.3% [28]. This substantial decrease of viscosity depends on the surface temperature as well as the Weber number.

4. Conclusions

The present study conducted extensive experiments for DI-water and xanthan gum droplets impinging on a heated copper surface and analyzed the effects of Weber numbers and surface temperatures on the dynamic spreading and receding behaviors. The following conclusions can be drawn:

(1) For a non-Newtonian droplet with shear-thinning characteristics, the original U–K model failed to predict the maximum spreading diameter when compared to the experimental data, whereas the modified model was in good agreement. This indicates that the shear-thinning effect involved in the effective viscosity should be included when estimating the viscous dissipation energy.

(2) Meanwhile, the maximum spreading diameters and time required to reach the maximum spread decreased with increasing Weber number, which is associated with the kinetic energy of a droplet impinging on the surface. When a droplet impinged on the heated surface, the maximum spreading diameter slightly increased for a DI-water droplet, whereas it remained nearly constant for a non-Newtonian droplet. This supports the hypothesis that for a non-Newtonian droplet, there is scarcely a dependency of surface temperature on the liquid motion in the spreading regime. However, there was a drastic change in the diameter and dynamic contact angle in the receding regime, indicating that the temperature effect on the liquid viscosity significantly affected.

(3) For an effective analysis of the receding motion, the present study used the retraction rate concept for DI-water and xanthan gum droplets. For the DI-water droplet case, the retraction rate remained constant regardless of the Weber number; however, it was affected by the change in the surface temperature. In particular, the retraction rate of the xanthan gum droplet became smaller than that of DI-water droplet, but it increased with the Weber number as well as the surface temperature. It was concluded that for a non-Newtonian droplet, the shear-thinning effect and temperature dependency of viscosity are important factors that significantly affect the receding motion.

Acknowledgements

This work was supported by the Mid-career Researcher Program through the National Research Foundation of Korea (NRF) Grant, funded by the Ministry of Education, Science and Technology (MEST) (NRF-2011-0016837). This research was also supported by the Chung-Ang University Excellent Student Scholarship and the Human Resources Development of Korea Institute of Energy Technology Evaluation and Planning (KETEP) Grant funded by the Korea government Ministry of Knowledge Economy (No. 20114030200020).

References

[1] A.L. Yarin, Drop impact dynamics: splashing, spreading, receding, bouncing, Annu. Rev. Fluid Mech. 38 (2006) 159–192.
[2] J.B. Lee, S.H. Lee, Dynamic wetting and spreading characteristics of a liquid droplet impinging on hydrophobic textured surfaces, Langmuir 27 (2011) 6565–6573.
[3] I.V. Roisman, Inertia dominated drop collisions. II. An analytical solution of the Navier–Stokes equations for a spreading viscous film, Phys. Fluids 21 (2009) 052104.
[4] I.V. Roisman, L. Opfer, C. Tropea, M. Raessi, J. Mostaghimi, S. Chandra, Drop impact onto a dry surface: role of the dynamic contact angle, Colloids Surf. A. 322 (2008) 183–191.
[5] I.V. Roisman, E. Berberović, C. Tropea, Inertia dominated drop collisions. I. On the universal flow in the lamella, Phys. Fluids 21 (2009) 052103.
[6] A. Alizadeh, V. Baidakov, S. Zhong, W. Shang, R. Li, J. Ruud, et al., Temperature dependent droplet impact dynamics on flat and textured surfaces, Appl. Phys. Lett. 100 (2012) 111601.
[7] M. Pasandideh-Fard, S.D. Aziz, S. Chandra, J. Mostaghimi, Cooling effectiveness of a water drop impinging on a hot surface, Int. J. Heat Fluid Fl. 22 (2001) 201–210.
[8] D. Chatzikyriakou, S.P. Walker, C.P. Hale, G.F. Hewitt, The measurement of heat transfer from hot surfaces to non-wetting droplets, Int. J. Heat Mass Trans. 54 (2011) 1432–1440.
[9] G. Strotos, M. Gavaises, G. Aleksis, K.S. Nikas, N. Nikolopoulos, A. Theodorakakos, Non-dimensionalisation parameters for predicting the cooling effectiveness of droplets impinging on moderate temperature solid surfaces, Int. J. Therm. Sci. 50 (2011) 698–711.

[10] G. Strotos, M. Gavaises, A. Theodorakakos, G. Bergeles, Numerical investigation of the cooling effectiveness of a droplet impinging on a heated surface, Int. J. Heat Mass Trans. 51 (2008) 4728–4742.
[11] E.S.R. Negeed, M. Albeirutty, Y. Takata, Dynamic behavior of micrometric single water droplets impacting onto heated surfaces with TiO_2 hydrophilic coating, Int. J. Therm. Sci. 79 (2014) 1–17.
[12] E.S.R. Negeed, S. Hidaka, M. Kohno, Y. Takata, Effect of the surface roughness and oxidation layer on the dynamic behavior of micrometric single water droplets impacting onto heated surfaces, Int. J. Therm. Sci. 70 (2013) 65–82.
[13] E.S.R. Negeed, S. Hidaka, M. Kohno, Y. Takata, High speed camera investigation of the impingement of single water droplets on oxidized high temperature surfaces, Int. J. Therm. Sci. 63 (2013) 1–14.
[14] E.S.R. Negeed, N. Ishihara, K. Tagashira, S. Hidaka, M. Kohno, Y. Takata, Experimental study on the effect of surface conditions on evaporation of sprayed liquid droplet, Int. J. Therm. Sci. 49 (2010) 2250–2271.
[15] V. Bergeron, D. Bonn, J.Y. Martin, L. Vovelle, Controlling droplet deposition with polymer additives, Nature 405 (2000) 772–775.
[16] S.M. An, S.Y. Lee, Observation of the spreading and receding behavior of a shear-thinning liquid drop impacting on dry solid surfaces, Exp. Therm. Fluid Sci. 37 (2012) 37–45.
[17] S.M. An, S.Y. Lee, Maximum spreading of a shear-thinning liquid drop impacting on dry solid surfaces, Exp. Therm. Fluid Sci. 38 (2012) 140–148.
[18] D. Bartolo, A. Boudaoud, G. Narcy, D. Bonn, Dynamics of non-Newtonian droplets, Phys. Rev. Lett. 99 (2007) 174502.
[19] D. Bartolo, C. Josserand, D. Bonn, Retraction dynamics of aqueous drops upon impact on non-wetting surfaces, J. Fluid Mech. 545 (2005) 329–338.
[20] J.H. Moon, J.B. Lee, S.H. Lee, Dynamic behavior of non-Newtonian droplets impinging on solid surfaces, Mater. Trans. 54 (2013) 260–265.
[21] G. German, V. Bertola, Impact of shear-thinning and yield-stress drops on solid substrates, J. Phys.: Condens. Matter. 21 (2009) 375111.
[22] V. Bertola, Drop impact on a hot surface: effect of a polymer additive, Exp. Fluids 37 (2004) 653–664.
[23] A. Dechelette, P.E. Sojka, C.R. Wassgren, Non-Newtonian drops spreading on a flat surface, J. Fluids Eng. 132 (2010) 101302.
[24] V. Bertola, An experimental study of bouncing Leidenfrost drops: Comparison between Newtonian and viscoelastic liquids, Int. J. Heat Mass Trans. 52 (2009) 1786–1793.
[25] E. Berberović, I.V. Roisman, S. Jakirlić, C. Tropea, Inertia dominated flow and heat transfer in liquid drop spreading on a hot substrate, Int. J. Heat Fluid Fl. 32 (2011) 785–795.
[26] T. Mao, D. Kuhn, H. Tran, Spread and rebound of liquid droplets upon impact on flat surfaces, AIChE J. 43 (1997) 2169–2179.
[27] B.B. Lee, E.-S. Chan, P. Ravindra, T.A. Khan, Surface tension of viscous biopolymer solutions measured using the du Nouy ring method and the drop weight methods, Polym. Bull. 69 (2012) 471–489.
[28] J. Kestin, M. Sokolov, W.A. Wakeham, Viscosity of liquid water in the range −8°C to 150°C, J. Phys. Chem. Ref. Data 7 (1978) 941–948.
[29] A.F. Stalder, T. Melchior, M. Müller, D. Sage, T. Blu, M. Unser, Low-bond axisymmetric drop shape analysis for surface tension and contact angle measurements of sessile drops, Colloids Surf. A. 364 (2010) 72–81.
[30] H.S. Ahn, J. Kim, M.H. Kim, Investigation of pool boiling critical heat flux enhancement on a modified surface through the dynamic wetting of water droplets, J. Heat Trans. 134 (2012) 071504.
[31] G. Son, Numerical simulation of microdroplet impact and evaporation on a solid surface, J. Heat Trans. 134 (2012) 101502.
[32] M. Gavaises, G. Strotos, A. Theodorakakos, G. Bergeles, Numerical investigation on the evaporation of droplets depositing on heated surfaces at low Weber numbers, Int. J. Heat Mass Trans. 51 (2008) 1516–1529.
[33] G. Strotos, N. Nikolopoulos, K.S. Nikas, K. Moustris, Cooling effectiveness of droplets at low Weber numbers: effect of temperature, Int. J. Therm. Sci. 72 (2013) 60–72.
[34] S.W. Park, B.S. Choi, K.W. Song, K.J. Oh, J.W. Lee, Absorption of carbon dioxide into aqueous xanthan gum solution containing monoethanolamine, Separ. Sci. Technol. 42 (2007) 3537–3554.
[35] N.B. Wyatt, H. Sirringhaus, M.W. Liberatore, T. Kawase, R.H. Friend, T. Shimoda, et al., High-resolution inkjet printing of all-polymer transistor circuits, Science 290 (2000) 2123–2126.
[36] M. Pasandideh-Fard, Y.M. Qiao, S. Chandra, J. Mostaghimi, Capillary effects during droplet impact on a solid surface, Phys. Fluid 8 (1996) 650.
[37] C. Ukiwe, D.Y. Kwok, On the maximum spreading diameter of impacting droplets on well-prepared solid surfaces, Langmuir 21 (2005) 666–673.
[38] I.V. Roisman, R. Rioboo, C. Tropea, Normal impact of a liquid drop on a dry surface: Model for spreading and receding, Proc. R. Soc. Lond. A. 458 (2002) 1411–1430.
[39] D.C. Vadillo, A. Soucemarianadin, C. Delattre, D.C.D. Roux, Dynamic contact angle effects onto the maximum drop impact spreading on solid surfaces, Phys. Fluid 21 (2009) 122002.
[40] S. Šikalo, C. Tropea, E. Ganić, Dynamic wetting angle of a spreading droplet, Exp. Therm. Fluid Sci. 29 (2005) 795–802.
[41] E. Choppe, F. Puaud, T. Nicolai, L. Benyahia, Rheology of xanthan solutions as a function of temperature, concentration and ionic strength, Carbonhyd. Polym. 82 (2010) 1228–1235.